Variable kinematic plate elements coupled via Arlequin method

Terms of use:

Publisher copyright

(Article begins on next page)

25 April 2024

Variable kinematic plate elements coupled via Arlequin method

F. Biscani[1], G. Giunta [1,*,†], S. Belouettar [1], E. Carrera[2] and H. Hu[3]

[1] *Centre de Recherche Public Henri Tudor, 29, av. John F. Kennedy, L-1855, Kirchberg, Luxembourg, Luxembourg*
[2] *Politecnico di Torino, 24, c.so Duca degli Abruzzi, 10129, Turin, Italy*
[3] *School of Civil Engineering, Wuhan University, 8, South Road of East Lake, Wuchang, 430072 Wuhan, China*

1. INTRODUCTION

Multi-layered structures are increasingly used in aerospace, automotive and ship vehicles. Nowadays, there are examples of fighter and commercial aircrafts, helicopters and gliders whose structure is entirely made of composite materials. The analysis and design of composite and sandwich structures is a cumbersome subject. In order to achieve an effective design, the mechanics of multi-layered structures should be modelled as accurately as possible. The drawback of refined plate theories or three-dimensional analyses is represented by the computational costs. The objective of the present work is to develop a consistent numerical method for the multiple models analysis of plates by means of variable kinematic models. Thanks to this approach, refined theories with higher accuracy and computational cost are adopted only in specific sub-domains where low-order theories are inaccurate. The remaining parts of the plate are then modelled using computationally cheap elements. The Arlequin method (see Ben Dhia [1–3] and Ben Dhia and Rateau [4]) is adopted to couple the sub-domains. A brief discussion on refined plate models and computational techniques to combine different domains follows.

In the case of bending mechanics, classical two-dimensional models are represented by classical lamination theory (CLT) see Kirchhoff [5], and first-order shear deformation theory (FSDT), see Reissner [6] and Mindlin [7]. Classical theories yield accurate results only in the case of thin plates and low degree of anisotropy. Many refinements of classical models have been proposed to

---
*Correspondence to: Gaetano Giunta, Department of Advanced Materials and Structures, Centre de Recherche Public Henri Tudor, 29, av. John F. Kennedy, L-1855, Kirchberg, Luxembourg, Luxembourg.

†E-mail: gaetano.giunta@tudor.lu

overcome the limitations of classical theories and to include partially or completely the so called C_z^0 requirements (see Carrera [8]). Both displacements and transverse stresses are C^0-class functions along the thickness direction: they have, in the most general case, discontinuous first derivatives at each interface where the mechanical properties change. The fulfilment of the C^0 requirements is a crucial point of multi-layered structures' two-dimensional modelling. A complete and exhaustive discussion of several contributions that appeared in literature has been covered by many state-of-the-art articles. Among these, the reviews proposed by Kapania and Raciti [9, 10], Noor and Burton [11], Reddy and Robbins [12], Carrera [13] and Hu et al. [14] should be mentioned. A unified formulation (UF) of axiomatically refined plate models was proposed by Carrera [15]. Models formulated on the basis of the Principle of Virtual Displacements (PVD) and Reissner's Mixed Variational Theorem [16] (RMVT) were both considered. Both equivalent single layer (ESL) and layer-wise (LW) approaches were adopted. CLT and FSDT models were retrieved as particu-lar cases. Through a concise notation for the unknowns field, problem governing equations were reduced to a 'fundamental nucleo' that does not depend upon the approximation order that is a free parameter of the formulation. A comprehensive assessment of the corresponding finite elements was addressed in Carrera [17].

As far as coupling of 'refined' and 'coarse' sub-domains of a structure is concerned, several numerical methods have been formulated in the last years. In such a manner, accurate results can be obtained with reduced computational costs. In the multi-grid method (see Fish et al. [18]), coarse and fine meshes share information inside an iterative algorithm. In the case of multiple models methods, structure's sub-domains may differ in the kinematic assumptions. In the s-version method (see Fish [19] and Fish and Markolefas [20]), incompatible meshes (different element size and polynomial order) with a local–global border are coupled. Park and Felippa [21] presented a continuum-based variational principle for the formulation of discrete governing equations of parti-tioned structural systems, including coupled substructures as well as sub-domains obtained by mesh decomposition. Another variational approach for coupling kinematically incompatible structural models was presented by Blanco et al. [22]. In the three-field formulation by Brezzi and Marini [23], an additional grid at the interface is introduced. The unknowns are represented independently in each sub-domain and on the interface, the matching being provided by suitable Lagrange multipliers. Ben Dhia et al. [1–4] proposed the Arlequin method. The coupling among different numerical models is obtained through Lagrange multipliers. This method was adopted by Hu et al. [24, 25] for the linear and non-linear analysis of sandwich beams modelled via one-dimensional and two-dimensional finite elements and by Biscani et al. [26] for the linear analysis of beams in the framework of UF: ESL beam elements of different orders, formulated via the principle of virtual displacements, are coupled. Reddy and Robbins [12] and Reddy [27] presented a multiple mod-els method on the basis of a variable kinematic theory and on mesh superposition in the sense of Fish [19] and Fish and Markolefas [20]. Coupling is obtained by linking the FSDT variables, which are present in all the considered models, without using Lagrangian multipliers. In contrast with the Arlequin method, total superposition is required in the case of non-conforming meshes.

In the present work, the Arlequin method is formulated in the context of Carrera's UF. Cou-pling between a large variety of models is considered. Main unknowns to be coupled differ in type, description approach and approximation order. Arlequin coupling matrix is obtained in the framework of UF in terms of a fundamental nucleo, whose expression depends only on the choice of the coupling operator. Refined elements are employed in the portion of the structure in which low-order theories would yield inaccurate results, for instance, where the stress field is quasi-three-dimensional. This approach, already presented for beam structures in Biscani et al. [26], is here extended to multi-layered plates. The novelty of the present work consists in consider-ing, besides ESL displacement-based models, also LW theories and mixed models with transverse stresses as primary variables. Several numerical investigations are also carried out to evaluate the influence of length parameter, weight parameter and extension of the superposition zone on the accuracy of the coupling. Non-conforming meshes are not considered. The proposed approach is validated towards mono-model UF theories as well as three-dimensional exact solutions. The total number of degrees of freedom and, therefore, the computational cost have been reduced, being the results still accurate.

2. PRELIMINARIES

A plate is a flat three-dimensional structure in which one dimension (its thickness) is negligible if compared to the in-plane dimensions. A Cartesian reference system is used. Plate's reference or middle plane Ω lies in the xy-plane, midway between top and bottom faces. The z-coordinate is along the through-the-thickness axis. Multi-layered plates of uniform thickness h are considered. The displacement field in a kth layer is

$$\mathbf{u}^{k\mathrm{T}}(x, y, z) = \left\{ \begin{array}{ccc} u_x^k(x, y, z) & u_y^k(x, y, z) & u_z^k(x, y, z) \end{array} \right\} \tag{1}$$

in which u_x, u_y and u_z are the displacement components along x-axis, y-axis and z-axis. Superscript 'T' represents the transposition operator. Bold letters denote arrays.

Stress, $\boldsymbol{\sigma}^k$, and strain, $\boldsymbol{\varepsilon}^k$, vectors in a kth layer are split into vectors $\boldsymbol{\sigma}_p^k$ and $\boldsymbol{\varepsilon}_p^k$ acting on planes parallel to Ω:

$$\boldsymbol{\sigma}_p^{k\mathrm{T}} = \left\{ \begin{array}{ccc} \sigma_{xx}^k & \sigma_{yy}^k & \sigma_{xy}^k \end{array} \right\} \quad \boldsymbol{\varepsilon}_p^{k\mathrm{T}} = \left\{ \begin{array}{ccc} \varepsilon_{xx}^k & \varepsilon_{yy}^k & \gamma_{xy}^k \end{array} \right\} \tag{2}$$

and $\boldsymbol{\sigma}_n^k$ and $\boldsymbol{\varepsilon}_n^k$ acting on planes perpendicular to Ω:

$$\boldsymbol{\sigma}_n^{k\mathrm{T}} = \left\{ \begin{array}{ccc} \sigma_{xz}^k & \sigma_{yz}^k & \sigma_{zz}^k \end{array} \right\} \quad \boldsymbol{\varepsilon}_n^{k\mathrm{T}} = \left\{ \begin{array}{ccc} \gamma_{xz}^k & \gamma_{yz}^k & \varepsilon_{zz}^k \end{array} \right\} \tag{3}$$

In the case of small displacements with respect to a characteristic dimension (h), linear relations between strain and displacement components hold. A compact vectorial notation can be adopted:

$$\boldsymbol{\varepsilon}_{p\mathrm{G}}^k = \boldsymbol{D}_p \boldsymbol{u}^k$$
$$\boldsymbol{\varepsilon}_{n\mathrm{G}}^k = (\boldsymbol{D}_{n\Omega} + \boldsymbol{D}_{nz})\boldsymbol{u}^k \tag{4}$$

Subscript 'G' denotes strains computed through geometrical relations. $\mathbf{D}_{n\Omega}$, $\mathbf{D}_{nz}$ and $\mathbf{D}_p$ are the following differential matrix operators:

$$\mathbf{D}_{n\Omega} = \begin{bmatrix} 0 & 0 & \frac{\partial}{\partial x} \\ 0 & 0 & \frac{\partial}{\partial y} \\ 0 & 0 & 0 \end{bmatrix} \quad \mathbf{D}_{nz} = \mathbf{I}\frac{\partial}{\partial z} \quad \mathbf{D}_p = \begin{bmatrix} \frac{\partial}{\partial x} & 0 & 0 \\ 0 & \frac{\partial}{\partial y} & 0 \\ \frac{\partial}{\partial y} & \frac{\partial}{\partial x} & 0 \end{bmatrix} \tag{5}$$

$\mathbf{I}$ is the unit matrix.

Under the hypothesis of linear elastic materials, generalised Hooke's law holds. According to Equations (2) and (3) and for a reference system not coincident with the orthotropic axes, it reads as follows:

$$\boldsymbol{\sigma}_{p\mathrm{C}}^k = \tilde{\boldsymbol{C}}_{pp}^k \boldsymbol{\varepsilon}_{p\mathrm{G}}^k + \tilde{\boldsymbol{C}}_{pn}^k \boldsymbol{\varepsilon}_{n\mathrm{G}}^k$$
$$\boldsymbol{\sigma}_{n\mathrm{C}}^k = \tilde{\boldsymbol{C}}_{np}^k \boldsymbol{\varepsilon}_{p\mathrm{G}}^k + \tilde{\boldsymbol{C}}_{nn}^k \boldsymbol{\varepsilon}_{n\mathrm{G}}^k \tag{6}$$

where subscript 'C' denotes field variables computed through the constitutive relations. $\tilde{\boldsymbol{C}}_{pp}^k$, $\tilde{\boldsymbol{C}}_{pn}^k$, $\tilde{\boldsymbol{C}}_{np}^k$ and $\tilde{\boldsymbol{C}}_{nn}^k$ are the following material stiffness matrices:

$$\tilde{\boldsymbol{C}}_{pp}^k = \begin{bmatrix} \tilde{C}_{11}^k & \tilde{C}_{12}^k & \tilde{C}_{16}^k \\ \tilde{C}_{12}^k & \tilde{C}_{22}^k & \tilde{C}_{26}^k \\ \tilde{C}_{16}^k & \tilde{C}_{26}^k & \tilde{C}_{66}^k \end{bmatrix} \quad \tilde{\boldsymbol{C}}_{pn}^k = \tilde{\boldsymbol{C}}_{np}^{k\mathrm{T}} = \begin{bmatrix} 0 & 0 & \tilde{C}_{13}^k \\ 0 & 0 & \tilde{C}_{23}^k \\ 0 & 0 & \tilde{C}_{36}^k \end{bmatrix} \quad \tilde{\boldsymbol{C}}_{nn}^k = \begin{bmatrix} \tilde{C}_{55}^k & \tilde{C}_{45}^k & 0 \\ \tilde{C}_{45}^k & \tilde{C}_{44}^k & 0 \\ 0 & 0 & \tilde{C}_{33}^k \end{bmatrix}$$
$$\tag{7}$$

For the sake of brevity, stiffness terms $\tilde{C}_{ij}^k$ as a function of the engineering constants are not reported here. For more details, see Reddy [27]. In the case of a first-order expansion or classical models, material stiffness coefficients should be reduced according to the plane stress condition as follows:

$$\tilde{Q}_{11}^k = \tilde{C}_{11}^k - \frac{\tilde{C}_{13}^{k^2}}{\tilde{C}_{33}^k} \quad \tilde{Q}_{22}^k = \tilde{C}_{22}^k - \frac{\tilde{C}_{23}^{k^2}}{\tilde{C}_{33}^k} \quad \tilde{Q}_{12}^k = \tilde{C}_{12}^k - \frac{\tilde{C}_{13}^k \tilde{C}_{23}^k}{\tilde{C}_{33}^k} \tag{8}$$

in order to avoid the thickness locking; see Carrera and Brischetto [28]. For mixed models, in which both displacements $\boldsymbol{u}$ and transverse shear/normal stresses $\boldsymbol{\sigma_n}$ are *a priori* variables according to RMVT, Hooke's equations should be rewritten as follows:

$$
\begin{aligned}
\boldsymbol{\sigma}_{p\mathrm{C}}^k &= \hat{\boldsymbol{C}}_{pp}^k \boldsymbol{\varepsilon}_{p\mathrm{G}}^k + \hat{\boldsymbol{C}}_{pn}^k \boldsymbol{\sigma}_{n\mathrm{M}}^k \\
\boldsymbol{\varepsilon}_{n\mathrm{C}}^k &= \hat{\boldsymbol{C}}_{np}^k \boldsymbol{\varepsilon}_{p\mathrm{G}}^k + \hat{\boldsymbol{C}}_{nn}^k \boldsymbol{\sigma}_{n\mathrm{M}}^k
\end{aligned}
\tag{9}
$$

where 'M' indicates that the out-of-plane stresses are *a priori* assumed and, therefore, modelled. The new stiffness matrices are

$$\hat{\boldsymbol{C}}_{pp}^k = \tilde{\boldsymbol{C}}_{pp}^k - \tilde{\boldsymbol{C}}_{pn}^k \tilde{\boldsymbol{C}}_{nn}^{k^{-1}} \tilde{\boldsymbol{C}}_{np}^k \quad \hat{\boldsymbol{C}}_{pn}^k = \hat{\boldsymbol{C}}_{np}^{k\mathrm{T}} = \tilde{\boldsymbol{C}}_{pn}^k \tilde{\boldsymbol{C}}_{nn}^{k^{-1}} \quad \hat{\boldsymbol{C}}_{nn}^k = \tilde{\boldsymbol{C}}_{nn}^{k^{-1}} \tag{10}$$

3. UNIFIED FORMULATION FOR PLATE MODELS

Two-dimensional modelling of plate structures consists of the separation of a generic unknown $\boldsymbol{a} = \boldsymbol{a}(x, y, z)$ into a set of thickness functions F_τ depending only upon the through-the-thickness coordinate z and the correspondent variables $\boldsymbol{a}_\tau$ depending upon the in-plane coordinates (x and y). The UF by Carrera [15] allows obtaining several two-dimensional models thanks to the following compact form:

$$\boldsymbol{a}(x, y, z) = F_\tau(z)\boldsymbol{a}_\tau(x, y) \tag{11}$$

where, according to Einstein's notation, τ is a dummy index standing for summation of $N + 1$ terms in which N is the through-the-thickness expansion order. In this work, N is assumed to be as high as 4. Thanks to the compact notation in Equation (11), the governing equations can be written in terms of a fundamental nucleo that does not depend formally upon N and the unknowns description. This latter can be ESL or LW. The primary unknowns can be displacements (PVD-based models) or both displacements and transverse stresses (mixed models based on RMVT).

3.1. Equivalent single layer theories

Via an ESL description, problem's unknowns are assumed globally for the whole structure. The unknown field is approximated as follows:

$$\boldsymbol{a} = F_0 \boldsymbol{a}_0 + F_1 \boldsymbol{a}_1 + \cdots + F_N \boldsymbol{a}_N = F_\tau \boldsymbol{a}_\tau, \quad \tau = 0, 1, \ldots, N \tag{12}$$

Within UF, MacLaurin's polynomials are adopted as thickness functions F_τ:

$$F_\tau = z^\tau \tag{13}$$

The choice of MacLaurin's polynomials allows obtaining classical theories such as CLT and FSDT as particular cases of a linear theory by (i) imposing a constant value of the transverse displacement through the thickness direction and, in the case of CLT, (ii) preventing out-of-plane shear deformations by assuming fictitiously high values of the material out-of-plane shear modulus. For more

details, see Carrera and Giunta [29]. Reduced material stiffness coefficients according to a plane stress condition, as shown in Equation (8), should be adopted in the case of classical theories and ESL first order theory.

3.2. Layer-wise theories

According to Reddy [27], in LW theories, unknowns are considered independently in a generic kth layer:

$$\boldsymbol{a^k} = F_t \boldsymbol{a_t^k} + F_b \boldsymbol{a_b^k} + F_l \boldsymbol{a_l^k} = F_\tau \boldsymbol{a_\tau^k} \ , \qquad \begin{array}{l} \tau = t, b, l \\ l = 2, \ldots, N \end{array} \tag{14}$$

Subscripts t and b stands for kth layer top and bottom values, and l denotes the higher-order terms of the through-the-thickness expansion. The thickness functions are a linear combination of Legendre's polynomials (see Carrera [17]), and they vary versus a local through-the-thickness dimensionless coordinate ζ_k:

$$\zeta_k = \frac{2z_k}{h_k} \tag{15}$$

being z_k a kth layer local coordinate and h_k its thickness. These thickness functions have the following properties:

$$\begin{aligned} \zeta_k = 1: & \quad F_t = 1, \quad F_b = 0, \quad F_l = 0 \\ \zeta_k = -1: & \quad F_t = 0, \quad F_b = 1, \quad F_l = 0 \end{aligned} \tag{16}$$

In LW mixed models, these properties ensure compatibility and equilibrium at layers' interfaces. $\boldsymbol{C_z^0}$ requirements are fulfilled: displacement and transverse stresses are continuous at layers' interfaces, and their first derivatives may be discontinuous.

3.3. Variational statements

The governing equations can be derived according to displacement-based or mixed variational statements. The PVD is used for the case of displacement-based models. For a laminate made of N_l layers, the PVD reads as follows:

$$\sum_{k=1}^{N_l} \int_{\Omega_k} \int_{h_k} \left(\delta \boldsymbol{\varepsilon}_{pG}^{kT} \boldsymbol{\sigma}_{pC}^k + \delta \boldsymbol{\varepsilon}_{nG}^{kT} \boldsymbol{\sigma}_{nC}^k \right) \mathrm{d}\Omega_k \mathrm{d}z = \sum_{k=1}^{N_l} \delta L_e^k \tag{17}$$

The integration domain Ω_k indicates the reference plane of each lamina. δ represents a virtual variation. L_e^k is the expression of the external work that accounts for an external load acting on a generic k layer.

Reissner's Mixed Variational Theorem is adopted when both displacements and transverse shear and normal stresses are *a priori* variables; see Reissner [16, 30]. RMVT is obtained via the addition of a Lagrange's multiplier that allows modelling the transverse stress vector $\boldsymbol{\sigma_n}$:

$$\sum_{k=1}^{N_l} \int_{\Omega_k} \int_{h_k} \left[\delta \boldsymbol{\varepsilon}_{pG}^{kT} \boldsymbol{\sigma}_{pC}^k + \delta \boldsymbol{\varepsilon}_{nG}^{kT} \boldsymbol{\sigma}_{nM}^k + \delta \boldsymbol{\sigma}_{nM}^{kT} \left(\boldsymbol{\varepsilon}_{nG}^k - \boldsymbol{\varepsilon}_{nC}^k \right) \right] \mathrm{d}\Omega_k \mathrm{d}z = \sum_{k=1}^{N_l} \delta L_e^k \tag{18}$$

3.4. Acronyms system

The following acronyms system is adopted for addressing the two-dimensional models that can be obtained via UF. The first letter indicates the approximation approach, and it can be either 'E' for an ESL approach or 'L' for an LW one. The second letter refers to the main unknowns: 'D' stands for displacement-based models and 'M' for mixed theories. A number indicates the order of

expansion. For instance, 'ED1'–'ED4' are linear to fourth-order ESL displacement-based models, whereas 'LD1'–'LD4' and 'LM1'–'LM4' are linear to fourth-order displacement-based and mixed LW models, respectively. ESL mixed models are not considered in the present work.

4. FINITE ELEMENT FORMULATION

The generic unknown a_τ^k is expressed in terms of the nodal unknowns $q_{\tau i}^{k\mathrm{T}}$ and the shape functions N_i (see Bathe [31]):

$$a_\tau^k(x, y) = N_i(x, y)q_{\tau i}^k, \quad i = 1, 2, \ldots, N_n \tag{19}$$

N_n denotes the element nodes number. Via substitution of Equation (19) into Equation (12) (ESL models) or Equation (14) (LW models), the following expression is obtained:

$$a^k(x, y, z) = F_\tau(z)N_i(x, y)q_{\tau i}^k \tag{20}$$

The formulation of RMVT-based elements is addressed in detail. Both displacements and transverse shear and normal stresses are modelled as primary unknowns:

$$q_{\tau i}^{k\mathrm{T}} = \left\{ q_{u\tau i}^{k\mathrm{T}}, q_{\sigma\tau i}^{k\mathrm{T}} \right\} = \left\{ \left\{ q_{u_x\tau i}^k, q_{u_y\tau i}^k, q_{u_z\tau i}^k \right\}, \left\{ q_{\sigma_{zz}\tau i}^k, q_{\sigma_{xz}\tau i}^k, q_{\sigma_{yz}\tau i}^k \right\} \right\} \tag{21}$$

where $q_{u\tau i}^{k\mathrm{T}}$ is the nodal displacements vector and $q_{\sigma\tau i}^{k\mathrm{T}}$ is the nodal transverse stresses vector. Because of the finite-element (FE) discretisation, the geometrical relations in Equation (4) read as follows:

$$\begin{aligned} \boldsymbol{\varepsilon}_{p\mathrm{G}}^k &= F_\tau \boldsymbol{D}_p (N_i \boldsymbol{I}) q_{u\tau i}^k \\ \boldsymbol{\varepsilon}_{n\mathrm{G}}^k &= F_\tau \boldsymbol{D}_{n\Omega} (N_i \boldsymbol{I}) q_{u\tau i}^k + F_{\tau,z} N_i q_{u\tau i}^k \end{aligned} \tag{22}$$

Subscripts preceded by comma represent differentiation. Upon substitution of Equations (22), (20) and (9) into Equation (18), the internal virtual work for a kth layer can be rewritten in the following compact form:

$$\delta L_i^k = \delta q_{\tau i}^{k\mathrm{T}} \boldsymbol{K}^{k\tau sij} q_{sj}^k \tag{23}$$

where $\boldsymbol{K}^{k\tau sij} \in \mathbb{R}^{6\times 6}$ is the fundamental nucleo of the FE stiffness matrix. According to the nodal vector unknowns separation in Equation (21), Equation (23) reads:

$$\delta L_i^k = \delta q_{u\tau i}^{k\mathrm{T}} \left(\boldsymbol{K}_{uu}^{k\tau sij} q_{usj}^k + \boldsymbol{K}_{u\sigma}^{k\tau sij} q_{\sigma sj}^k \right) + \delta q_{\sigma\tau i}^{k\mathrm{T}} \left(\boldsymbol{K}_{\sigma u}^{k\tau sij} q_{usj}^k + \boldsymbol{K}_{\sigma\sigma}^{k\tau sij} q_{\sigma sj}^k \right) \tag{24}$$

where the following arrays in $\mathbb{R}^{3\times 3}$:

$$\begin{aligned} \boldsymbol{K}_{uu}^{k\tau sij} &= \triangleleft \boldsymbol{D}_p^{\mathrm{T}} (N_i \boldsymbol{I}) \, \boldsymbol{Z}_{pp}^{k\tau s} \boldsymbol{D}_p (N_j \boldsymbol{I}) \triangleright_{\Omega_k} \\ \boldsymbol{K}_{u\sigma}^{k\tau sij} &= \triangleleft \boldsymbol{D}_p^{\mathrm{T}} (N_i \boldsymbol{I}) \, \boldsymbol{Z}_{pn}^{k\tau s} (N_i \boldsymbol{I}) N_j + \boldsymbol{D}_{n\Omega}^{\mathrm{T}} (N_i \boldsymbol{I}) \, E^{\tau s} N_j + E^{\tau,z s} N_i N_j \boldsymbol{I} \triangleright_{\Omega_k} \\ \boldsymbol{K}_{\sigma u}^{k\tau sij} &= \triangleleft N_i E^{\tau s} \boldsymbol{D}_{n\Omega} (N_j \boldsymbol{I}) + E^{\tau s,z} N_i N_j \boldsymbol{I} - N_i \boldsymbol{Z}_{np}^{k\tau s} \boldsymbol{D}_p (N_j \boldsymbol{I}) \triangleright_{\Omega_k} \\ \boldsymbol{K}_{\sigma\sigma}^{k\tau sij} &= \triangleleft - N_i \boldsymbol{Z}_{nn}^{k\tau s} N_j \triangleright_{\Omega_k} \end{aligned} \tag{25}$$

represent the sub-block components of $\boldsymbol{K}^{k\tau sij}$. Symbol $\triangleleft \cdots \triangleright_{\Omega_k}$ denotes the integral on Ω_k. Subscripts τ and s count the expansion terms along the thickness direction, whereas subscripts i

and j range over the element nodes number. The generic term $\mathbf{Z}_{\eta\zeta}^{k\tau_{(,z)}s_{(,z)}}$ is a through-the-thickness layer integral accounting for material and geometric stiffness:

$$
\begin{aligned}
\mathbf{Z}_{\eta\zeta}^{k\tau_{(,z)}s_{(,z)}} &= \hat{\mathbf{C}}_{\eta\zeta}^{k} E^{\tau_{(,z)}s_{(,z)}} \quad \eta, \zeta = p, n \\
E^{\tau_{(,z)}s_{(,z)}} &= \int_{h_k} F_{\tau_{(,z)}} F_{s_{(,z)}} \mathrm{d}z
\end{aligned}
\tag{26}
$$

As far as the whole structure is concerned, the FEM problem in the framework of the proposed UF is governed by the following equation:

$$
\delta \overline{\mathbf{q}}_{\tau i}^{k}: \quad \overline{\mathbf{K}}^{k\tau sij} \overline{\mathbf{q}}_{sj}^{k} = \overline{\mathbf{P}}_{\tau i}^{k}
\tag{27}
$$

where $\overline{\mathbf{K}}^{k\tau sij}$ and $\overline{\mathbf{q}}_{sj}^{k}$ are the global FE stiffness matrix and nodal unknowns vector. $\overline{\mathbf{P}}_{\tau i}^{k}$ is a loading vector that is variationally coherent to the mechanical model through the external work. In the case of RMVT-based elements, Equation (27) reads as follows:

$$
\begin{aligned}
\delta \overline{\mathbf{q}}_{u\tau i}^{k\mathrm{T}}: &\quad \overline{\mathbf{K}}_{uu}^{k\tau sij} \overline{\mathbf{q}}_{usj}^{k} + \overline{\mathbf{K}}_{u\sigma}^{k\tau sij} \overline{\mathbf{q}}_{\sigma sj}^{k} = \overline{\mathbf{P}}_{u\tau i}^{k} \\
\delta \overline{\mathbf{q}}_{\sigma\tau i}^{k\mathrm{T}}: &\quad \overline{\mathbf{K}}_{\sigma u}^{k\tau sij} \overline{\mathbf{q}}_{usj}^{k} + \overline{\mathbf{K}}_{\sigma\sigma}^{k\tau sij} \overline{\mathbf{q}}_{\sigma sj}^{k} = 0
\end{aligned}
\tag{28}
$$

where the stiffness matrix and the load vector are partitioned according to the separation of primary unknowns in displacements and stresses.

Principle of Virtual Displacements based elements can be obtained in a similar manner as the RMVT-based ones where $\mathbf{q}_{\tau i}^{k\mathrm{T}} = \mathbf{q}_{u\tau i}^{k\mathrm{T}}$ and $\mathbf{K}^{k\tau sij} \in \mathbb{R}^{3\times3}$:

$$
\begin{aligned}
\mathbf{K}^{k\tau sij} = \vartriangleleft \mathbf{D}_{p}^{\mathrm{T}} (N_i \mathbf{I}) \left[\mathbf{Z}_{pp}^{k\tau s} \mathbf{D}_{p} (N_j \mathbf{I}) + \mathbf{Z}_{pn}^{k\tau s} \mathbf{D}_{n\Omega} (N_j \mathbf{I}) + \mathbf{Z}_{pn}^{k\tau s,z} N_j \right] + \\
+ \mathbf{D}_{n\Omega}^{\mathrm{T}} (N_i \mathbf{I}) \left[\mathbf{Z}_{np}^{k\tau s} \mathbf{D}_{p} (N_j \mathbf{I}) + \mathbf{Z}_{nn}^{k\tau s} \mathbf{D}_{n\Omega} (N_j \mathbf{I}) + \mathbf{Z}_{nn}^{k\tau s,z} N_j \right] + \\
+ N_i \left[\mathbf{Z}_{np}^{k\tau,z s} \mathbf{D}_{p} (N_j \mathbf{I}) + \mathbf{Z}_{nn}^{k\tau,z s} \mathbf{D}_{n\Omega} (N_j \mathbf{I}) + \mathbf{Z}_{nn}^{k\tau,z s,z} N_j \right] \vartriangleright_{\Omega_k}
\end{aligned}
\tag{29}
$$

$\mathbf{Z}_{\eta\zeta}^{k\tau_{(,z)}s_{(,z)}}$ is computed using the generalised Hooke's law as in Equation (6), that is, $\tilde{\mathbf{C}}_{\eta\zeta}^{k}$ instead of $\hat{\mathbf{C}}_{\eta\zeta}^{k}$. The FEM problem of the whole structure reads as follows:

$$
\delta \overline{\mathbf{q}}_{u\tau i}^{k}: \quad \overline{\mathbf{K}}^{k\tau sij} \overline{\mathbf{q}}_{usj}^{k} = \overline{\mathbf{P}}_{u\tau i}^{k}
\tag{30}
$$

Demasi and Carrera [32] presented hybrid RMVT-based elements in which the *a priori* assumed stresses are eliminated at element level via a static condensation. Since the primary unknowns are only displacements, the element stiffness matrix has the same dimension as the one of a corresponding PVD-based element. In the present work, the full mixed implementation is retained. Four-node quadrilateral elements are considered. Shear locking is here avoided via a reduced integration scheme. Because four-node elements are used, only a Gauss point is considered in the numerical integration of the element shape functions N_i and their derivatives: all the terms in the fundamental nucleo of the FE stiffness matrix are reduced integrated.

5. ARLEQUIN METHOD IN THE CONTEXT OF THE UNIFIED FORMULATION

Plate's volume (V) is divided into two sub-domains A_1 and A_2 that are partially overlapped as shown in Figure 1. S represents the overlapping volume. For each sub-domain, a different model is assumed:

$$
\mathbf{a}_{\xi}^{k} = N_i F_{\tau_{\xi}} \mathbf{q}_{\tau_{\xi}i}^{k} \quad \text{with} \quad \tau_{\xi} = 1, 2, \ldots, N_u^{A_{\xi}}, \ \xi = 1, 2
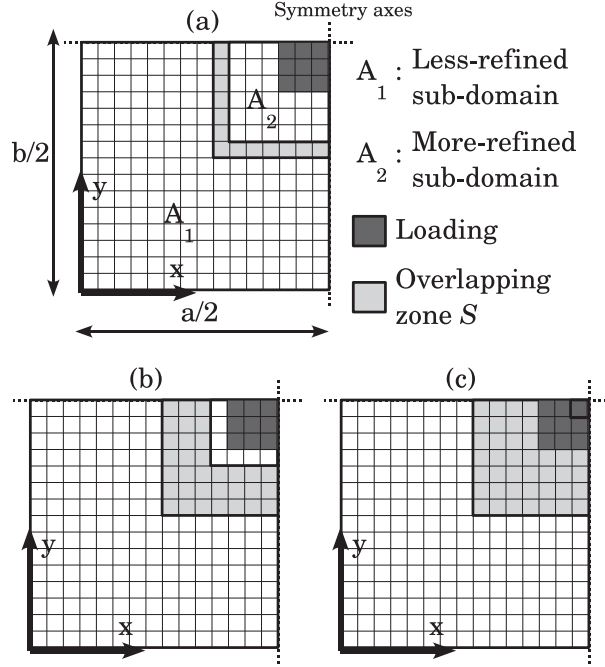\tag{31}
$$

Figure 1. Plate mesh, loading and sub-domains considering several superimposition zones: (a) minimum S^a, (b) reduced S^b and (c) extended S^c.

ξ being a dummy index that counts the sub-domains. The global mechanical problem is solved merging together the two sub-domains via the Arlequin method. The internal and external virtual works are computed for each sub-domain. The structural integrity in the overlapping volume is ensured via a Lagrangian multiplier field ($\boldsymbol{\lambda}$) and a coupling operator (C_ξ) that links the DOF of each sub-domain within the overlapping volume. The variational statement becomes

$$\sum_{k=1}^{N_l} \left(\delta L_{i\xi}^k + \delta L_{c\xi}^k \right) = \sum_{k=1}^{N_l} \delta L_{e\xi}^k \tag{32}$$

$\delta L_{i\xi}^k$ is the virtual variation of the strain energy in each sub-domain. In the case of RMVT-based models, $\delta L_{i\xi}^k$ is

$$\sum_{k=1}^{N_l} \delta L_{i\xi}^k = \sum_{k=1}^{N_l} \int_{A_\xi} \alpha_\xi \left[\delta\boldsymbol{\varepsilon}_{pG}^{kT} \boldsymbol{\sigma}_{pC}^k + \delta\boldsymbol{\varepsilon}_{nG}^{kT} \boldsymbol{\sigma}_{nM}^k + \delta\boldsymbol{\sigma}_{nM}^{kT} \left(\boldsymbol{\varepsilon}_{nG}^k - \boldsymbol{\varepsilon}_{nC}^k \right) \right] \mathrm{d}V_k \text{ with } \begin{cases} \alpha_\xi = 1 \text{ in } A_\xi \setminus S \\ \alpha_1 + \alpha_2 = 1 \text{ in } S \end{cases}$$
$$\tag{33}$$

α_ξ are weighting functions for scaling the energy in each sub-domain in order to not consider the energy in the overlapping volume twice. According to Ben Dhia and Rateau [4], α_ξ should be such that the sub-domain with a more refined description has a higher weight in the global equilibrium. The virtual external work $\delta L_{e\xi}^k$ is treated in a similar manner.

$\delta L_{c\xi}^k$ is the virtual coupling work:

$$\delta L_{c\xi}^k = (-1)^\xi \, \delta C_\xi^k \left(\delta\boldsymbol{\lambda}^k, \boldsymbol{u}_\xi^k \right) \tag{34}$$

Two coupling operators are considered (see Ben Dhia and Rateau [4] and Guidault and Belytschko [33]):

- L^2 coupling:

$$\delta C_\xi^k = \int_{S_\xi^k} \delta \boldsymbol{\lambda}^{k\mathrm{T}} \boldsymbol{u}_\xi^k \, \mathrm{d}V_k \tag{35}$$

- H^1 coupling:

$$\delta C_\xi^k = \int_{S_\xi^k} \left\{ \delta \boldsymbol{\lambda}^{k\mathrm{T}} \boldsymbol{u}_\xi^k + \tilde{l}^2 \left[\boldsymbol{\varepsilon}_{p\mathrm{G}}^{k\mathrm{T}} \left(\delta \boldsymbol{\lambda}^k \right) \boldsymbol{\varepsilon}_{p\mathrm{G}}^k \left(\boldsymbol{u}_\xi^k \right) + \boldsymbol{\varepsilon}_{n\mathrm{G}}^{k\mathrm{T}} \left(\delta \boldsymbol{\lambda}^k \right) \boldsymbol{\varepsilon}_{n\mathrm{G}}^k \left(\boldsymbol{u}_\xi^k \right) \right] \right\} \, \mathrm{d}V_k \tag{36}$$

S_ξ^k is the volume of the kth layer in the overlapping region. $\tilde{l}$ is a real parameter representative of a characteristic length. $\boldsymbol{\varepsilon}(\boldsymbol{\lambda})$ is defined in the same manner as the mechanical strain $\boldsymbol{\varepsilon}(\boldsymbol{u}_\xi)$ where the Lagrangian multiplier field is used instead of the displacement one. Stress components are not accounted for by these two coupling operators. Ben Dhia [3] proved that L^2 coupling operator is meaningless for the continuous Arlequin problem. In the discrete problem, it can be considered as an approximation of a dual Lagrange field linked to a dual continuous Arlequin coupling. The Lagrangian multiplier field is discretised according to the UF:

$$\boldsymbol{\lambda}^k = N_i F_{\tau_\lambda} \boldsymbol{\Lambda}_{\tau_\lambda i}^k \tag{37}$$

where $\boldsymbol{\Lambda}_{\tau_\lambda i}^k$ is the nodal unknown vector. The virtual work for a kth layer is derived coherently to Equation (23) via substitution of Equation (37) into Equation (35) or (36):

$$\delta C_\xi^k = \delta \boldsymbol{\Lambda}_{\tau_\lambda i}^{k\mathrm{T}} \mathbf{C}_\xi^{k\tau_\lambda s_\xi ij} \boldsymbol{q}_{u s_\xi j}^k \tag{38}$$

$\mathbf{C}_\xi^{k\tau_\lambda s_\xi ij}$ is the fundamental nucleo of the coupling matrix. In the case of L^2 coupling, this is diagonal, and its components are

$$C_{\xi mn}^{k\tau_\lambda s_\xi ij} = \delta_{mn} E_{\tau_\lambda s_\xi}^k \triangleleft N_i N_j \triangleright_\Omega \quad \text{with } m, n = 1, 2, 3 \tag{39}$$

where δ_{mn} is Kronecker's delta. Terms $E_{\tau_\lambda s_\xi}^k$ are defined as

$$E_{\tau_\lambda s_\xi}^k = \int_{h_k} F_{\tau_\lambda} F_{s_\xi} \, \mathrm{d}z \tag{40}$$

For the coupling operator H^1, coupling matrix fundamental nucleo can be obtained straightforwardly noticing that H^1 coupling operator is the sum of the L^2 one and a term similar to the virtual internal work in Equation (17). The components of this latter term are those of the stiffness matrix that correspond to the diagonal terms of the constitutive matrices $\tilde{\mathbf{C}}_{pp}$ and $\tilde{\mathbf{C}}_{nn}$:

$$C_{11}^{k\tau_\lambda s_\xi ij} = C_{22}^{k\tau_\lambda s_\xi ij} = C_{33}^{k\tau_\lambda s_\xi ij} = E_{\tau_\lambda s_\xi}^k \triangleleft N_i N_j \triangleright_\Omega +$$

$$+ \tilde{l}^2 \left[E_{\tau_\lambda s_\xi}^k \left(\triangleleft N_{i,x} N_{j,x} \triangleright_\Omega + \triangleleft N_{i,y} N_{j,y} \triangleright_\Omega \right) + E_{\tau_{\lambda,z} s_{\xi,z}}^k \triangleleft N_i N_j \triangleright_\Omega \right]$$

$$C_{12}^{k\tau_\lambda s_\xi ij} = \tilde{l}^2 E_{\tau_\lambda s_\xi}^k \triangleleft N_{i,y} N_{j,x} \triangleright_\Omega \quad C_{13}^{k\tau_\lambda s_\xi ij} = \tilde{l}^2 E_{\tau_{\lambda,z} s_\xi}^k \triangleleft N_i N_{j,x} \triangleright_\Omega$$

$$C_{21}^{k\tau_\lambda s_\xi ij} = \tilde{l}^2 E_{\tau_\lambda s_\xi}^k \triangleleft N_{i,x} N_{j,y} \triangleright_\Omega \quad C_{23}^{k\tau_\lambda s_\xi ij} = \tilde{l}^2 E_{\tau_{\lambda,z} s_\xi}^k \triangleleft N_i N_{j,y} \triangleright_\Omega$$

$$C_{31}^{k\tau_\lambda s_\xi ij} = \tilde{l}^2 E_{\tau_\lambda s_{\xi,z}}^k \triangleleft N_{i,x} N_j \triangleright_\Omega \quad C_{32}^{k\tau_\lambda s_\xi ij} = \tilde{l}^2 E_{\tau_\lambda s_{\xi,z}}^k \triangleleft N_{i,y} N_j \triangleright_\Omega \tag{41}$$

where

$$E_{\tau_{\lambda(,y)(,z)} s_{\xi(,y)(,z)}}^k = \int_{h_k} F_{\tau_{\lambda(,y)(,z)}} F_{s_{\xi(,y)(,z)}} \, \mathrm{d}z \tag{42}$$

Coupling matrices are not affected by shear locking: full integration is adopted for the Lagrange multiplier shape functions N_i and their derivatives. According to Ben Dhia [2] and Guidault and Belytschko [33], the same approximation order should be assumed for the low-order model and the Lagrangian multiplier. This choice avoids a locking phenomenon that arises when the approximation of the more refined model is adopted for the discretisation of the Lagrangian multiplier field. Considering the whole structure and assuming that the refined model is adopted in the sub-domain A_2, the governing equations are

$$
\begin{bmatrix}
\overline{K}_{A_1\backslash S}^{\tau_1 s_1 ij} & 0 & 0 & 0 & 0 \\
0 & (1-\alpha)\,\overline{K}_{A_1\cap S}^{\tau_1 s_1 ij} & 0 & 0 & \overline{C}_1^{\tau_1 s_1 ij\,\mathrm{T}} \\
0 & 0 & \overline{K}_{A_2\backslash S}^{\tau_2 s_2 ij} & 0 & 0 \\
0 & 0 & 0 & \alpha\overline{K}_{A_2\cap S}^{\tau_2 s_2 ij} & -\overline{C}_2^{\tau_2 s_1 ij\,\mathrm{T}} \\
0 & \overline{C}_1^{\tau_1 s_1 ij} & 0 & -\overline{C}_2^{\tau_2 s_1 ij} & 0
\end{bmatrix}
\left\{
\begin{array}{c}
\overline{q}_{s_1 j}^{A_1\backslash S} \\
\overline{q}_{s_1 j}^{A_1\cap S} \\
\overline{q}_{s_2 j}^{A_2\backslash S} \\
\overline{q}_{s_2 j}^{A_2\cap S} \\
\overline{\Lambda}_{s_\lambda j}
\end{array}
\right\} =
$$
$$
=
\left\{
\begin{array}{c}
\overline{P}_{\tau_1 i}^{A_1\backslash S} \\
(1-\alpha)\,\overline{P}_{\tau_1 i}^{A_1\cap S} \\
\overline{P}_{\tau_2 i}^{A_2\backslash S} \\
\alpha\overline{P}_{\tau_2 i}^{A_2\cap S} \\
0
\end{array}
\right\}
\tag{43}
$$

where overlined terms refer to the whole structure. In the case of a PVD-based model, Equation (33) reads as follows:

$$
\sum_{k=1}^{N_l} \delta L_{i\xi}^k = \sum_{k=1}^{N_l} \int_{A_\xi} \alpha_\xi \left(\delta \boldsymbol{\varepsilon}_{pG}^{k\mathrm{T}} \boldsymbol{\sigma}_{pC}^k + \delta \boldsymbol{\varepsilon}_{nG}^{k\mathrm{T}} \boldsymbol{\sigma}_{nC}^k \right) \mathrm{d}V_k \quad \text{with} \quad \left\{ \begin{array}{l} \alpha_\xi = 1 \text{ in } A_\xi \backslash S \\ \alpha_1 + \alpha_2 = 1 \text{ in } S \end{array} \right.
\tag{44}
$$

Assuming that a refined RMVT-based model is adopted in the sub-domain A_2, whereas sub-domain A_1 is modelled via PVD-based elements, Equation (43) is rewritten as

$$
\begin{bmatrix}
\overline{K}_{A_1\backslash S}^{\tau_1 s_1 ij} & 0 & 0 & 0 & 0 & 0 & 0 \\
0 & (1-\alpha)\,\overline{K}_{A_1\cap S}^{\tau_1 s_1 ij} & 0 & 0 & 0 & 0 & \overline{C}_1^{\tau_1 s_1 ij\,\mathrm{T}} \\
0 & 0 & \overline{K}_{uuA_2\backslash S}^{\tau_2 s_2 ij} & \overline{K}_{u\sigma A_2\backslash S}^{\tau_2 s_2 ij} & 0 & 0 & 0 \\
0 & 0 & \overline{K}_{\sigma u A_2\backslash S}^{\tau_2 s_2 ij} & \overline{K}_{\sigma\sigma A_2\backslash S}^{\tau_2 s_2 ij} & 0 & 0 & 0 \\
0 & 0 & 0 & 0 & \alpha\overline{K}_{uuA_2\cap S}^{\tau_2 s_2 ij} & \alpha\overline{K}_{u\sigma A_2\cap S}^{\tau_2 s_2 ij} & -\overline{C}_2^{\tau_2 s_1 ij\,\mathrm{T}} \\
0 & 0 & 0 & 0 & \alpha\overline{K}_{\sigma u A_2\cap S}^{\tau_2 s_2 ij} & \alpha\overline{K}_{\sigma\sigma A_2\cap S}^{\tau_2 s_2 ij} & 0 \\
0 & \overline{C}_1^{\tau_1 s_1 ij} & 0 & 0 & -\overline{C}_2^{\tau_2 s_1 ij} & 0 & 0
\end{bmatrix}
\left\{
\begin{array}{c}
\overline{q}_{s_1 j}^{A_1\backslash S} \\
\overline{q}_{s_1 j}^{A_1\cap S} \\
\overline{q}_{us_2 j}^{A_2\backslash S} \\
\overline{q}_{\sigma s_2 j}^{A_2\backslash S} \\
\overline{q}_{us_2 j}^{A_2\cap S} \\
\overline{q}_{\sigma s_2 j}^{A_2\cap S} \\
\overline{\Lambda}_{s_\lambda j}
\end{array}
\right\} =
$$
$$
=
\left\{
\begin{array}{c}
\overline{P}_{\tau_1 i}^{A_1\backslash S} \\
(1-\alpha)\,\overline{P}_{\tau_1 i}^{A_1\cap S} \\
\overline{P}_{u\tau_2 i}^{A_2\backslash S} \\
0 \\
\alpha\overline{P}_{u\tau_2 i}^{A_2\cap S} \\
0 \\
0
\end{array}
\right\}
$$

6. NUMERICAL RESULTS AND DISCUSSION

Square plates having sides length a equal to 0.1 m are considered. The side-to-thickness ratio a/h is equal to 10. Relatively thick plates are, therefore, investigated. A localised transverse pressure (P) equal to 1 MPa is applied on a square region of side length equal to $a/5$ centred at point $(a/2, a/2, h/2)$ as shown in Figure 1. This configuration has been considered because the region close to the loading application is likely to present a three-dimensional stress field, and a refined model is required there. In the general case in which the location of a three-dimensional stress field cannot be determined *a priori*, refined sub-domains should be chosen on the basis of experience and
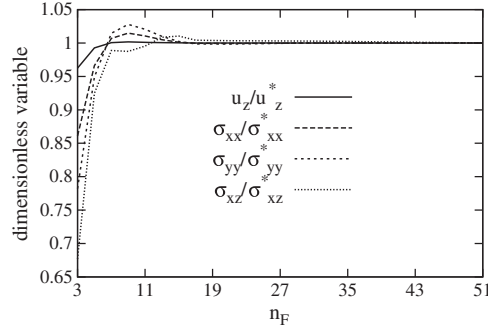
Figure 2. Convergence of Pagano's solution for a [0/90/0] plate. Starred results have been obtained with $n_F = 101$.
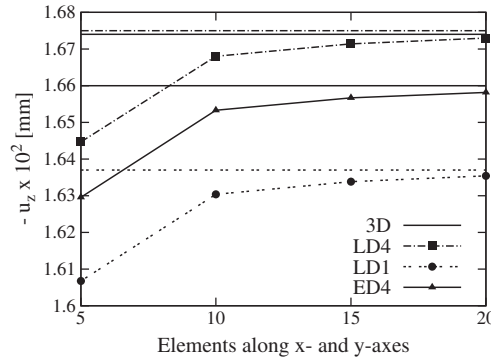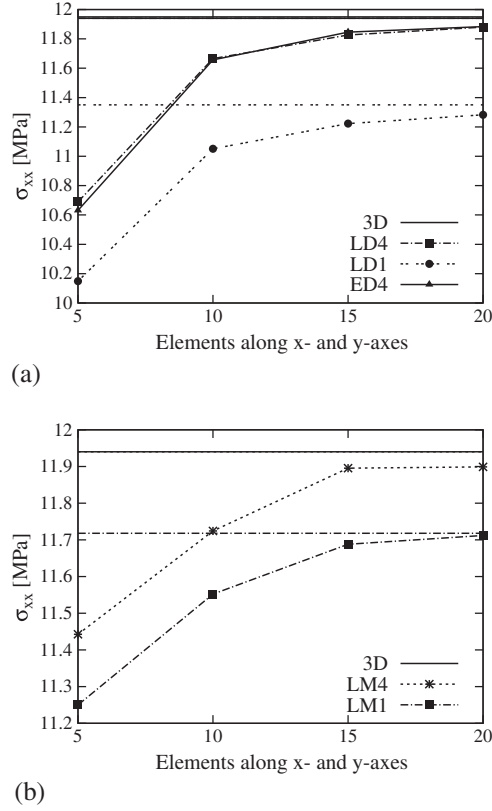

(a)
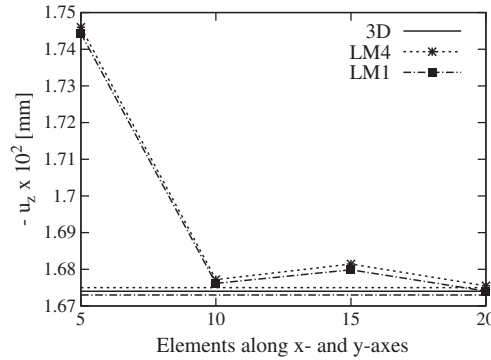
(b)

Figure 3. Convergence of the transverse displacement u_z versus the number of elements in the case of theories based on (a) the Principle of Virtual Displacements and (b) the Reissner's Mixed Variational Theorem. [0/90/0] stacking sequence. Horizontal lines without dots report the corresponding analytical solutions.

preliminary analyses via low-order models. A symmetric $[0/90/0]$ and an anti-symmetric $[90/0]_2$ stacking sequences are considered. The stacking sequence starts from the plate top. Ply angles are measured versus the x-axis. The layers are all made of the same orthotropic material, whose mechanical properties are $E_L = 1.325 \cdot 10^5$ MPa, $E_T = 1.08 \cdot 10^4$ MPa, $G_{LT} = 5.7 \cdot 10^3$ MPa, $G_{TT} = 3.4 \cdot 10^3$ MPa, $v_{LT} = 0.24$ and $v_{TT} = 0.49$. Four-node quadrilateral elements are employed. Because of the problem symmetry, only a quarter of the plate is modelled. Results are presented in terms of the transverse displacement u_z, in-plane normal stresses σ_{xx}, σ_{yy} and the out-of-plane

(a)

(b)

Figure 4. Convergence of the normal stress σ_{xx} versus the number of elements in the case of theories based on (a) the Principle of Virtual Displacements and (b) the Reissner's Mixed Variational Theorem. $[0/90/0]$ stacking sequence. Horizontal lines without dots report the corresponding analytical solutions.

Table I. Transverse displacement and stresses for the $[0/90/0]$ plate.

	$-10^5 \times u_z$ (m)		σ_{xx} (MPa)		σ_{yy} (MPa)		$-10 \times \sigma_{xz}$ (MPa)		DOF
3D	1.674		11.94		2.019		6.524		
	FE	AS	FE	AS	FE	AS	FE	AS	
LM4	1.681	1.675	11.89	11.94	1.993	2.020	6.523	6.540	19968
LD4	1.672	1.675	11.83	11.94	1.983	2.020	6.464	6.523	9984
LD1	1.634	1.637	11.22	11.35	2.102	2.142	6.422	6.519	3072
ED4	1.657	1.660	11.85	11.95	1.985	2.005	5.830	5.865	3840
ED1	1.587	1.609	10.38	10.44	1.604	1.852	3.872	3.813	1536
FSDT	1.605	1.609	10.33	10.44	1.826	1.852	3.872	3.813	1280
CLT	1.255	1.260	10.88	11.00	1.617	1.642	—	—	768

FE, finite-element solution; AS, analytical solution; FSDT, first-order shear deformation theory; CLT, classical lamination theory.

shear stress σ_{xz} Unless differently stated, u_z, σ_{xx} and σ_{yy} are evaluated at $(a/2, a/2, -h/2)$, and σ_{xz} is computed at $(5a/12, a/2, 0)$.

Mono-model solutions are first presented. The accuracy of the proposed theories is discussed showing the fulfilment of the C_z^0 requirements and the through-the-thickness equilibrium. The convergence of the solution versus the number of elements in the mesh is also investigated through comparison with the corresponding closed-form analytical solution and a three-dimensional exact solution based upon Pagano's solution [34]. The variable kinematic models are then addressed. Their accuracy is assessed towards the corresponding mono-model results and three-dimensional

Table II. Transverse displacement and stresses for the $[90/0]_2$ plate.

|	$-10^5 \times u_z$ (m)		σ_{xx} (MPa)		σ_{yy} (MPa)		$-10 \times \sigma_{xz}*$ (MPa)		$-10 \times \sigma_{xz}†$ (MPa)		DOF
3D	1.719		11.28		1.823		6.104		6.104		
	FE	AS	FE	AS	FE	AS	FE	AS	FE	AS	
LM4	1.725	1.719	11.23	11.28	1.807	1.824	6.141	6.121	6.141	6.121	26112
LD4	1.717	1.719	11.17	11.28	1.802	1.824	6.118	6.145	6.069	6.104	13056
LD1	1.692	1.694	10.78	10.91	1.909	1.931	5.263	5.297	6.308	6.376	3840
ED4	1.698	1.700	11.19	11.28	1.778	1.789	8.214	8.267	4.899	4.931	3840
ED2	1.600	1.644	9.429	9.741	1.476	1.544	5.484	5.465	3.271	3.260	2304
ED1	1.596	1.634	9.937	10.16	1.202	1.446	5.806	5.562	3.463	3.318	1536
FSDT	1.614	1.634	9.938	10.16	1.420	1.446	5.671	5.562	3.382	3.318	1280
CLT	1.323	1.344	9.812	10.03	1.406	1.431	—	—	—	—	768

FE, finite-element solution; AS, analytical solution; FSDT, first-order shear deformation theory; CLT, classical lamination theory.
*Value at the bottom of the second layer.
†Value at the top of the third layer.
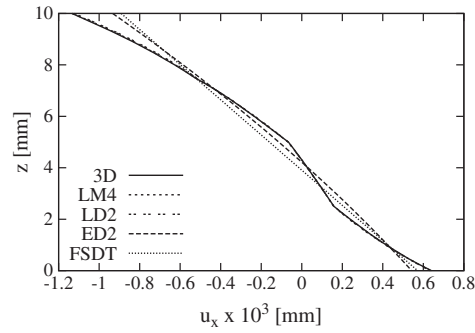
(a)
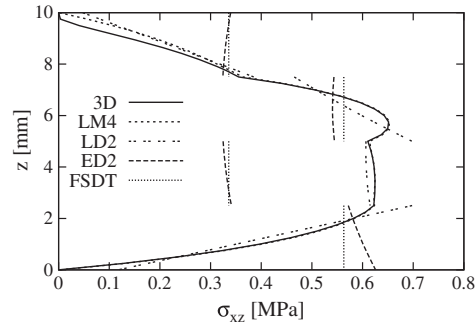
(b)

Figure 5. Through-the-thickness variation of (a) u_x and (b) σ_{xz} computed at $x/a = 5/12$, $y/a = 1/2$; $[90/0]_2$ plate.

exact solutions. The effect of the coupling operator, the extension of the superposition zone and the weight parameters are investigated.

6.1. Preliminary mono-model results

Pagano's three-dimensional solution is here extended in order to assess the accuracy of the UF models. The localised loading is approximated by a Fourier expansion, n_F being the number of harmonic terms along the x and y directions. The convergence of the transverse displacement u_z, in-plane normal stresses σ_{xx} and σ_{yy} and the out-of-plane shear stress σ_{xz} versus n_F is presented
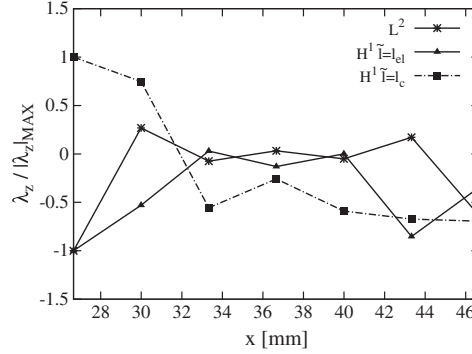
(a)
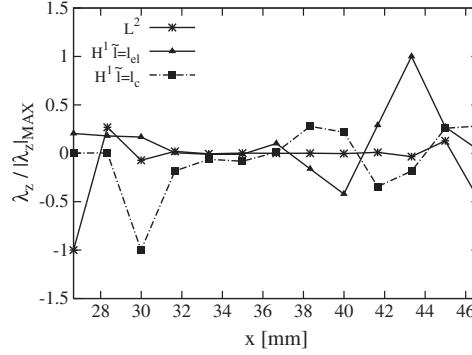
(b)

Figure 6. Variation of the Lagrangian multiplier λ_z along the x-axis in the overlapping region $x/a \in [4/15, 7/15]$ at $y/b = 1/2$ and $z = 0$ for a $[0/90/0]$ plate in the case of the coupling of two ED1 models with (a) mesh represented in Figure 1 and (b) refined mesh with halved elements' side length.
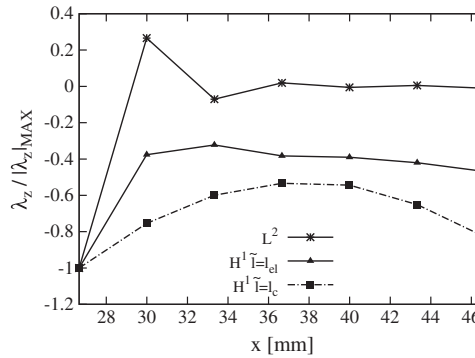
Figure 7. Variation of the Lagrangian multiplier λ_z along the x-axis in the overlapping region $x/a \in [4/15, 7/15]$ at $y/b = 1/2$ and $z = 0$ for a $[0/90/0]$ plate in the case of LD2–LD4-coupled solution.

15

in Figure 2. The symmetric [0/90/0] plate is considered. Results are normalised with respect to the values for $n_F = 101$. This latter value of n_F has been chosen in order to ensure a convergence of the shear stress with four significant digits.

As far as the proposed theories are concerned, the convergence of the transverse displacement u_z and the in-plane normal stresses σ_{xx} versus the number of elements are presented in Figures 3 and 4, respectively. FE results are compared to the analytical ones obtained by a Navier-type solution with $n_F = 101$ in the Fourier expansion of the loading. The transverse displacement u_z and the normal stresses σ_{xx} with a mesh of 15×15 elements differ from those with a mesh of 20×20 elements by less than 0.5%. A regular mesh of 15×15 elements is, therefore, adopted in the following analyses. Elements' sides length l_{el} is equal to $a/30$.

Transverse displacement and stresses for the symmetric [0/90/0] plate are reported in Table I. Results are computed via three-dimensional exact theory and both UF analytical (AS) and FE mono-model solutions. Higher-order LW analytical results match the three-dimensional reference solution.
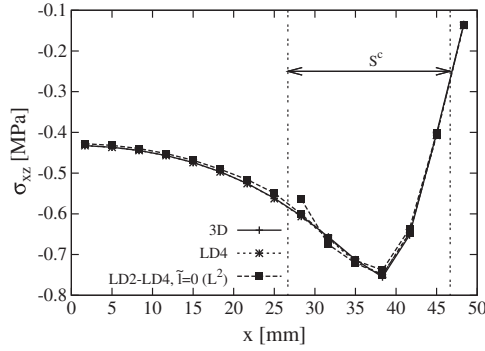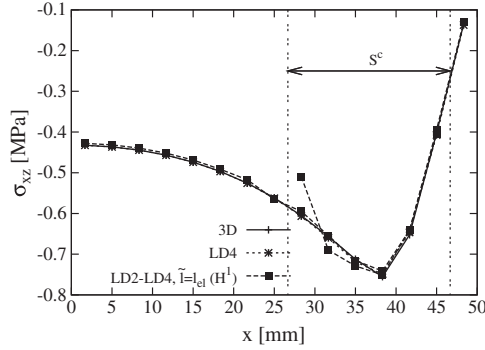

(a)

(b)

(c)
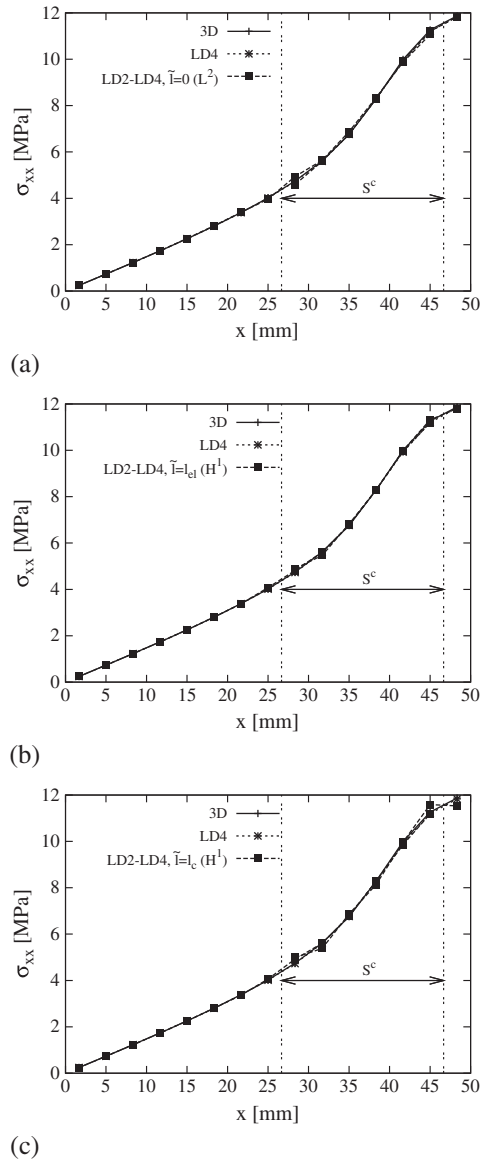
Figure 8. σ_{xx} along the x-axis for $y/b = 1/2$ at plate bottom for a [0/90/0] plate. LD2–LD4-coupled solution with (a) $\tilde{l} = 0$, (b) $\tilde{l} = l_{el}$ and (c) $\tilde{l} = l_c$.

ESL displacement-based models do not predict σ_{xz} accurately. As far as the FE solution is concerned, LM4 model yields results that differ from the reference solution by about 1%, at worst. In the case of transverse displacement predicted by ED1 theory, the error is about 6%. For the employed mesh, the difference in the transverse displacement between the FE solution and the corresponding analytical one is about 1.4%, at worst. The last column in Table I represents the number of DOF of the FE solution.

The case of an anti-symmetric $[90/0]_2$ plate is presented in Table II. As far as accuracy and convergence of the solutions are concerned, the same conclusions as for Table I are valid. The out-of-plane shear stress σ_{xz} is computed at both the bottom of the second layer and the top of the third one, in order to show that LW mixed models satisfy the through-the-thickness equilibrium.

(a)

(b)

(c)
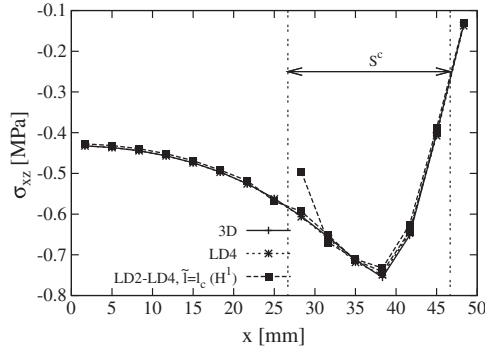
Figure 9. σ_{xz} along the x-axis for $y/b = 1/2$ at mid-plane for a $[0/90/0]$ plate. LD2–LD4-coupled solution with (a) $\tilde{l} = 0$, (b) $\tilde{l} = l_{\mathrm{el}}$ and (c) $\tilde{l} = l_c$.

The through-the-thickness variation of u_x and σ_{xz} is presented in Figure 5. The displacement component u_x is computed at $x/a = 5/12$, $y/b = 1/2$. C_z^0 requirements for displacements are satisfied by LW theories. The transverse shear stress continuity at the layers' interface is fulfilled by the RMVT-based theories.

6.2. Variable kinematic results

Finite elements that differ by the variables' description (ESL or LW), and the through-the-thickness expansion order are coupled. The coupling between PVD-based and RMVT-based elements is also addressed. Figure 1 presents the plate division into sub-domains and the mesh. Refined models are assumed for sub-domain A_2 that has been discretised via 49 elements. As shown in Figure 1, three different overlapping zone S are considered. They differ by the extensions along x-axis and y-axis. A sensitivity analysis is carried out in terms of (i) length parameter $\tilde{l}$, (ii) extension of the superposition zone, and (iii) weighting function α_ξ.

6.2.1. Length parameter Three values of $\tilde{l}$ are considered: zero, l_e and l_c. The latter is the length of the superposition zone along the x-axis or y-axis. It should be noticed that L^2 coupling operator can be considered as a particular case of H^1 one with $\tilde{l}$ equal to zero. The superposition zone as in Figure 1(c) and addressed as S^c is used. Such a large superposition zone, which includes most of the refined sub-domain, is not well suited for practical application of the Arlequin method. It is considered in the present work in order to highlight the spatial variation of quantities inside the overlapping volume. The coupling of two identical kinematic models ED1 is considered in the first place. According to Ben Dhia and Rateau [4], weighting functions equal to 0.5 are assumed. Figure 6 presents the Lagrangian multiplier λ_z along x-axis at $y/b = 1/2$ and $z = 0$ for a $[0/90/0]$ plate. Results are normalised versus their absolute maximum values $|\lambda_z|_{\text{MAX}}$. Two meshes are considered: the mesh shown in Figure 1(c) and a refined mesh with halved elements side length. As noticed in Ben Dhia and Rateau [4] and confirmed in Guidault and Belytschko [33], the coupling operator L^2 yields a multiplier field that tends to be singular on the interfaces of the superposition zone: the multiplier field is almost null everywhere except near the boundaries of the overlapping volume where it oscillates. If the elements' size is reduced, the oscillation regions become smaller. As explained by Ben Dhia [3], the multiplier field seems to converge up to a homogenisation factor to a surface-Lagrange multiplier. The transverse displacement, the normal in-plane stresses and the shear stresses match the case of mono-model solution regardless of the choice of the length parameter. For sake of brevity, they are not explicitly reported. In the second case, an LD2 model (sub-domain A_1) is coupled with an LD4 model (sub-domain A_2). According to Ben Dhia and Rateau [4] and unless differently stated, α_2 equal to 0.98 is used. Figure 7 presents the Lagrangian multiplier λ_z along x axis at $y/b = 1/2$ at mid-plane. For L^2, λ_z tends to be singular at the interface with the unrefined model. The distribution of σ_{xx} along the x-axis for $y/a = 1/2$ at plate bottom is shown in Figure 8.
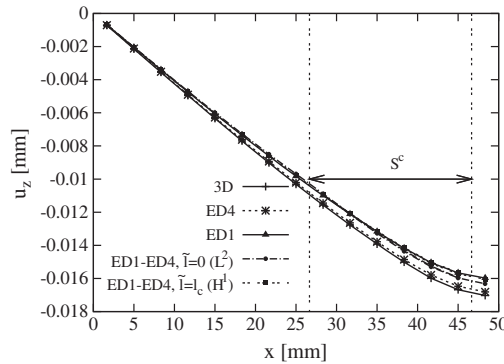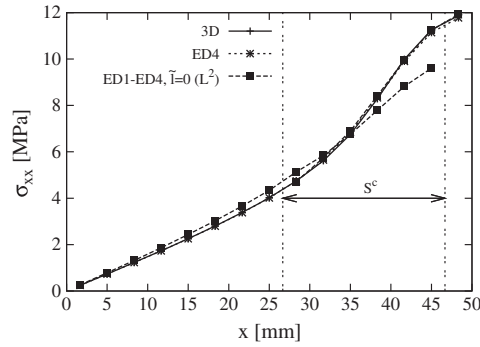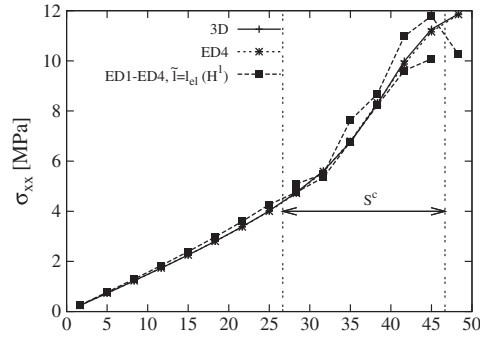

Figure 10. u_z along the x-axis for $y/b = 1/2$ at mid-plane for a $[0/90/0]$ plate. ED1–ED4-coupled solution.

The case $\tilde{l} = l_{\text{el}}$ yields the least perturbed solution, whereas for $\tilde{l} = l_c$ the oscillation in the coupling zone yields an underestimated value of σ_{xx} in the refined zone. Figure 9 presents the variation of σ_{xz} along x-axis. The shear stress is computed at $y/b = 1/2$ and $z = 0$. The variation of the length parameter affects the solution mainly in the coupling zone. It has been observed that the transverse displacement via LD2–LD4-coupled solution matches the corresponding mono-model one. It is not reported here for sake of brevity.

An ED1–ED4-coupled solution is also considered in order to investigate the coupling between lower and higher ESL theories. The transverse displacement along the x-axis for $y/a = 1/2$ at mid-plane is presented in Figure 10. Results for $\tilde{l} = l_{\text{el}}$ and $\tilde{l} = 0$ are very similar, and only the latter is, therefore, presented in the figure. The variable kinematic results are not very accurate because of the ED1 model in the coupled solution. The distribution of σ_{xx} is shown in Figure 11. L^2 coupling operator yields better results than the H^1 does. Similar considerations hold for the variation of σ_{xz}
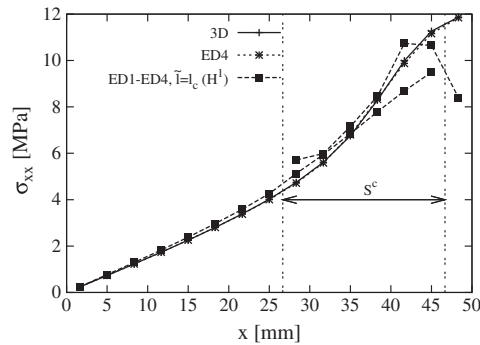
(a)

(b)

(c)

Figure 11. σ_{xx} along the x-axis for $y/b = 1/2$ at plate bottom for a $[0/90/0]$ plate. ED1–ED4-coupled solution with (a) $\tilde{l} = 0$, (b) $\tilde{l} = l_{\text{el}}$ and (c) $\tilde{l} = l_c$.

as shown in Figure 12. For both normal and shear stresses, results obtained with $\tilde{l} = l_{\mathrm{el}}$ are better than those obtained with $\tilde{l} = l_c$. In order to show the effect of the lower-order theory in the coupled solution, a plate made of aluminium ($E = 73$ GPa and $\nu = 0.34$) is investigated. All the other analysis parameters are unchanged. Stress components σ_{xx} and σ_{xz} are presented in Figures 13 and 14, respectively. ED1 model is more accurate when compared to the case of the composite plate. For the normal stress, no significant differences are found between the two coupling operators. In the case of the shear stress, results via H^1 coupling operator are smoother than the one through L^2.

The presented results confirm those reported by Ben Dhia and Rateau [4] and Guidault and Belytschko [33]: L^2 coupling operator presents a multiplier field that tends to be singular near the interfaces of the superposition zone. This is not the case for H^1, which yields a smoother multiplier field. When coupling identical kinematic models or models with similarly accurate kinematics,
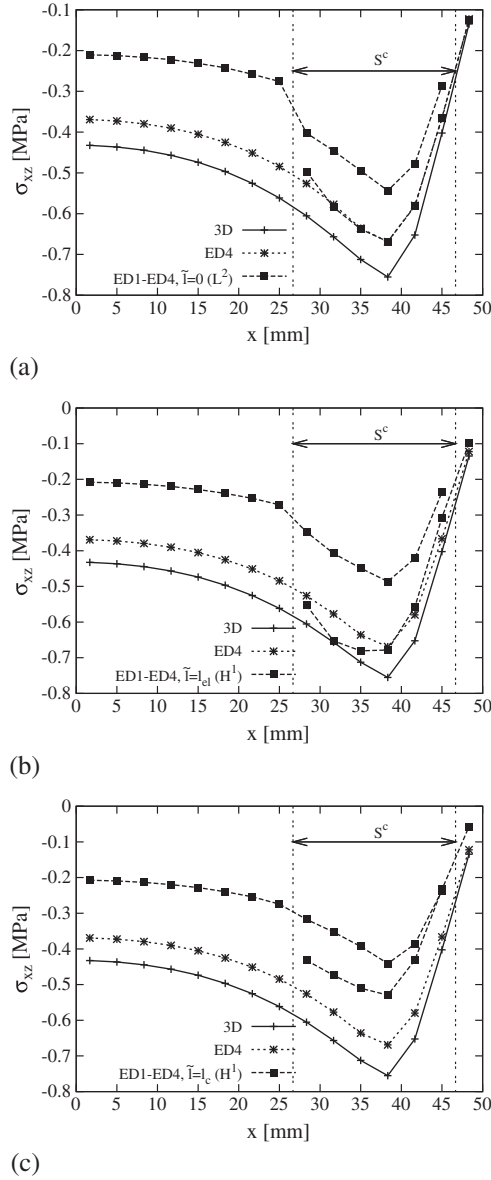

Figure 12. σ_{xz} along the x-axis for $y/b = 1/2$ at mid-plane for a $[0/90/0]$ plate. ED1–ED4-coupled solution with (a) $\tilde{l} = 0$, (b) $\tilde{l} = l_{\mathrm{el}}$ and (c) $\tilde{l} = l_c$.

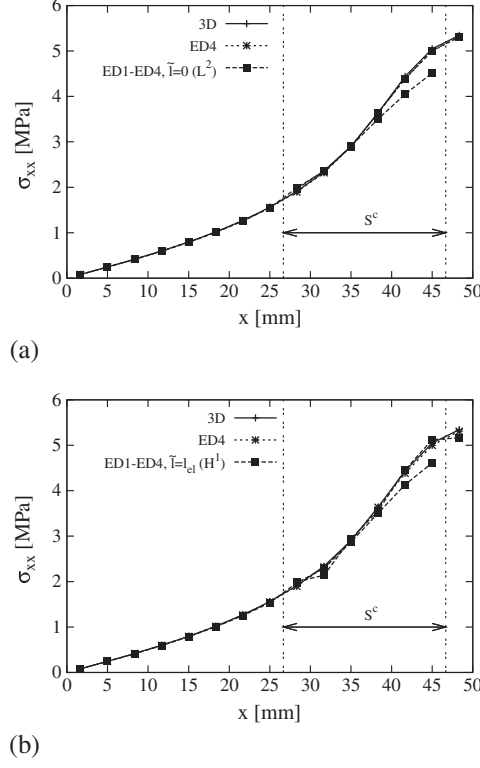Figure 13. σ_{xx} along the x-axis for $y/b = 1/2$ at plate bottom for an aluminium plate. ED1–ED4-coupled solution with (a) $\tilde{l} = 0$ and (b) $\tilde{l} = l_{\mathrm{el}}$.

results obtained via H^1 are similar to those by L^2. Nevertheless, in the considered cases, H^1 may yield inaccurate results if the unrefined theories are not appropriate to model the mechanics of the structure (especially when the transverse shear is important). This behaviour is emphasised by high values of $\tilde{l}$. The relation enforced by H^1 (see Guidault and Belytschko [33]) in the superposition zone is

$$(\boldsymbol{u}_1 - \boldsymbol{u}_2) - \tilde{l}^2 \left[\Delta \left(\boldsymbol{u}_1 \right) - \Delta \left(\boldsymbol{u}_2 \right) \right] = 0 \tag{46}$$

where Δ is the Laplacian. The higher the parameter $\tilde{l}$, the higher the contribution of the derivatives of the displacements in Equation (46). As shown in Table I, the ED1 model, especially for the prediction of the transverse shear stresses, is not accurate. The contribution due to the derivatives of strain components may introduce a disturbance in the superposition zone. L^2 couples only the displacements that are, in general, more accurate than the transverse strains in lower-order plate models.

6.2.2. Extension of the superposition zone The influence of the extension of the superposition zone on the coupling is investigated. Several superposition zones, as shown in Figure 1, are considered. Both L^2 and H^1 coupling operators are considered. For the latter case, a length parameter $\tilde{l}$ equal to l_{el} is considered. In order to avoid the perturbation in the coupling due to the plate theories, two refined models are coupled (ED3 model in sub-domain A_1 and LD4 model in A_2). Figure 15 present σ_{xx} and σ_{xz} in the case of L^2. The extension of the superposition zone does not affect the results in a significant manner. This conclusion is supported by the fact, as shown in Figure 7, that the Lagrangian multipliers' contribution is concentrated at the interface with the low-order model. The case of H^1 coupling is shown in Figure 16. For the considered cases, the effect of the size of the superposition zone is very small, the curves in the figures barely being distinguishable: the superposition zone does not affect significantly the accuracy of the solution. On the other side, the
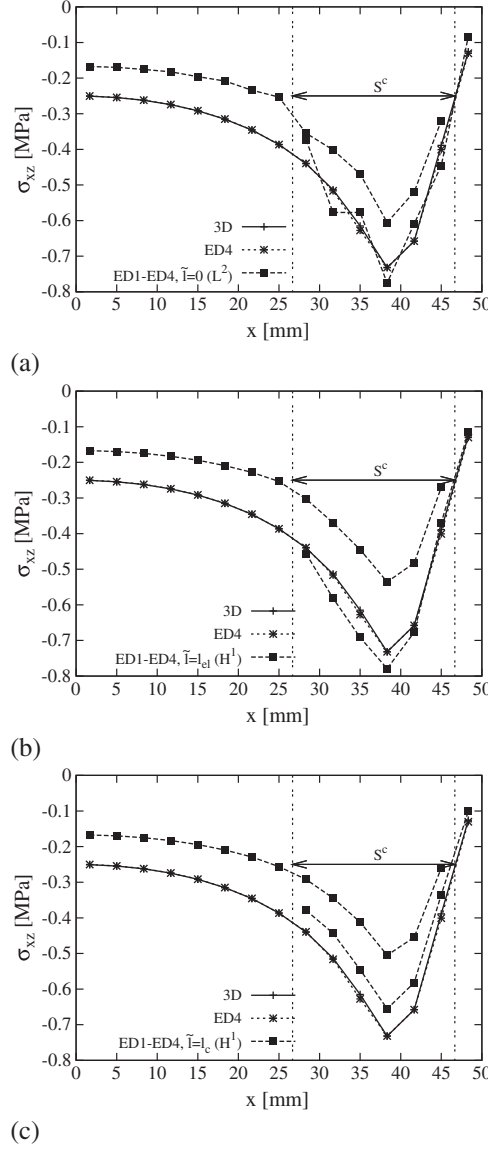
(a)

(b)

(c)

Figure 14. σ_{xz} along the x-axis for $y/b = 1/2$ at mid-plane for an aluminium plate. ED1–ED4-coupled solution with (a) $\tilde{l} = 0$, (b) $\tilde{l} = l_{\mathrm{el}}$ and (c) $\tilde{l} = l_c$.

bigger the extension of the superposition zone, the higher the number of DOF, and therefore, small superposition volumes should be used. The influence of the distance between the loading region and the superposition zone is considered in Figure 17. σ_{xz} in the case of H^1 coupling is presented. A load of 400 N is applied as a uniform transverse pressure on square regions centred at point $(a/2, a/2, h/2)$ with side lengths $a/3$, $a/5$ and $a/15$. Using the mesh in Figure 1, these regions correspond to 5×5, 3×3 and 1×1 elements, respectively. Superposition zone S^a is adopted. The smaller the loading application area, the higher the shear stress gradient. Multiple models solutions match the corresponding mono-model ones outside of the superposition zone regardless of the extension of the loading region. For the considered cases, this is also valid for displacements and normal stresses.

6.2.3. Weight parameters Three different values of α_2, the weight parameter of the refined model, are used: 0.02, 0.5 and 0.98. Superposition zone S^a is considered. A length parameter $\tilde{l}$ equal to zero and l_{el} is considered. An ED3 model is coupled to an LD4 model. The
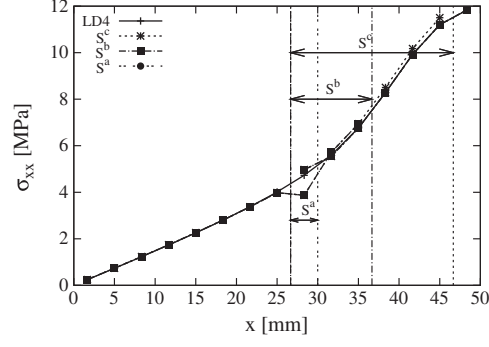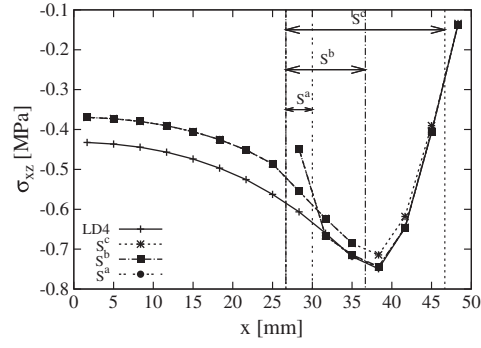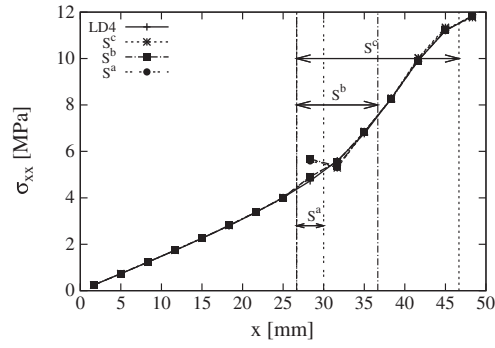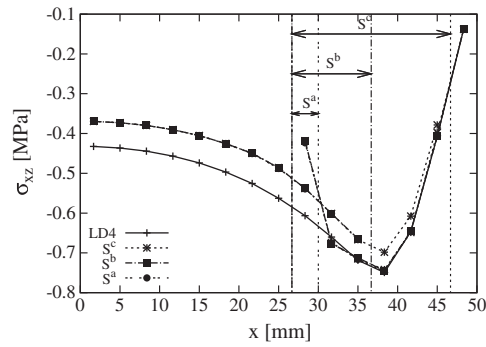
Figure 15. ED3–LD4 L^2 coupling for a [0/90/0] plate for different superposition volumes. (a) σ_{xx} at plate bottom and (b) σ_{xz} at mid-plane along the x-axis for $y/b = 1/2$.

Figure 16. ED3–LD4 H^1 coupling with $\tilde{l} = l_{\mathrm{el}}$ for a [0/90/0] plate for different superposition volumes. (a) σ_{xx} at plate bottom and (b) σ_{xz} at mid-plane along the x-axis for $y/b = 1/2$.

variation of σ_{xx} and σ_{xz} along the x-axis at $y/a = 1/2$ is presented in Figures 18 and 19, respectively. For the considered cases, H^1 coupling operator is more sensitive than the L^2 one to the weight parameters. The results confirm, as reported in Ben Dhia and Rateau [4], that the sub-domain with the most refined description should have a higher weight in the global equilibrium.

6.2.4. Different kinematics and variational principles Unified formulation models that differ in the type of the main unknowns, expansion order and approximation level (ESL or LW) are coupled. The coupling parameters are fixed coherently to the results already presented: (i) the smallest super-position zone S^a is used; (ii) higher weight in the global equilibrium is given to the most refined
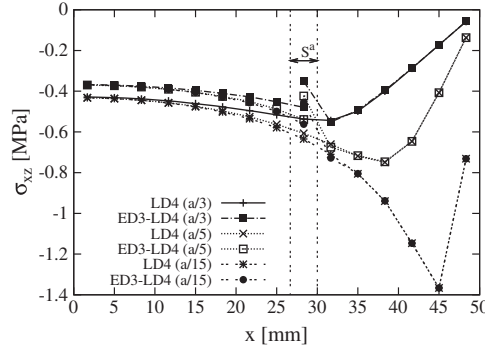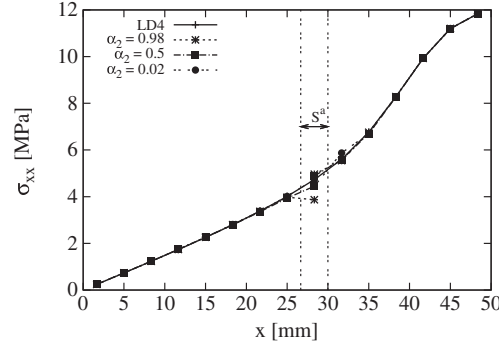

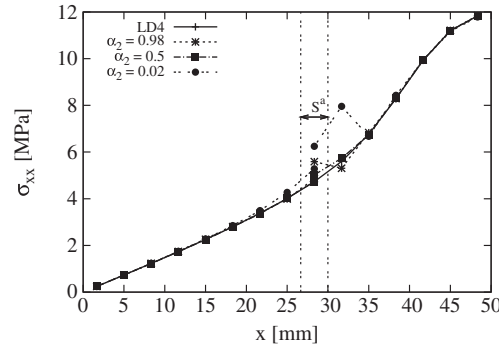Figure 17. σ_{xz} at mid-plane along the x-axis for $y/b = 1/2$ for a [0/90/0] plate. ED3–LD4 H^1 coupling with $\tilde{l} = l_{el}$ for loading regions with different side lengths.
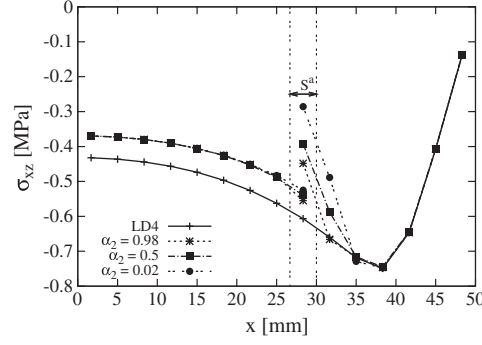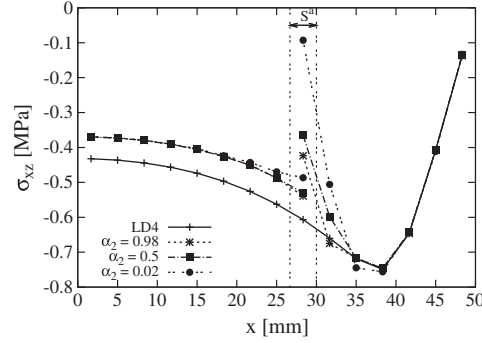

(a)

(b)

Figure 18. σ_{xx} along the x-axis for $y/b = 1/2$ at plate bottom for a [0/90/0] plate. ED3–LD4-coupled solution for different α_ξ with (a) $\tilde{l} = 0$ and (b) $\tilde{l} = l_{el}$.

Figure 19. σ_{xz} along the x-axis for $y/b = 1/2$ at mid-plane for a $[0/90/0]$ plate. ED3–LD4-coupled solution for different α_ξ with (a) $\tilde{l} = 0$ and (b) $\tilde{l} = l_{\rm el}$.

Table III. Transverse displacement and stresses for the $[0/90/0]$ plate, variable kinematic multiple models.

	$-10^5 \times u_z$ (m)	σ_{xx} (MPa)	σ_{yy} (MPa)	$-10 \times \sigma_{xz}$ (MPa)	DOF
L^2 coupling operator					
LD1–LM4	$1.658, -1.36^*$	$11.82, -0.58$	$1.975, -0.90$	$6.478, -0.69$	7968
ED4–LD4	$1.665, -0.41$	$11.83, +0.00$	$1.976, -0.35$	$6.465, +0.01$	6216
LD1–LD4	$1.660, -0.71$	$11.84, +0.08$	$1.977, -0.30$	$6.497, +0.51$	5472
ED1–LD4	$1.617, -3.28$	$11.91, +0.67$	$1.953, -1.51$	$6.481, +0.26$	3984
FSDT–LD4	$1.617, -3.28$	$11.91, +0.67$	$1.953, -1.51$	$6.481, +0.26$	3736
ED3–ED4	$1.657, +0.00$	$11.84, -0.08$	$1.985, +0.00$	$5.831, +0.01$	3936
ED1–ED4	$1.609, -2.89$	$11.92, +0.59$	$1.962, -1.15$	$5.848, +0.30$	2448
FSDT–ED4	$1.609, -2.89$	$11.92, +0.59$	$1.962, -1.15$	$5.848, +0.30$	2200
H^1 coupling operator					
LD1–LM4	$1.661, -1.19$	$11.81, -0.67$	$1.974, -0.95$	$6.490, -0.50$	7968
ED4–LD4	$1.666, -0.35$	$11.85, +0.16$	$1.978, -0.25$	$6.467, +0.04$	6216
LD1–LD4	$1.663, -0.58$	$11.85, +0.16$	$1.974, -0.45$	$6.485, +0.32$	5472
ED1–LD4	$1.620, -3.11$	$11.92, +0.76$	$1.953, -1.51$	$6.458, -0.09$	3984
FSDT–LD4	$1.620, -3.11$	$11.92, +0.76$	$1.953, -1.51$	$6.458, -0.09$	3736
ED3–ED4	$1.657, +0.00$	$11.84, -0.08$	$1.985, +0.00$	$5.832, +0.03$	3936
ED1–ED4	$1.611, -2.77$	$11.92, +0.59$	$1.963, -1.10$	$5.838, +0.13$	2448
FSDT–ED4	$1.611, -2.77$	$11.92, +0.59$	$1.963, -1.10$	$5.838, +0.13$	2200

*Percentage difference with respect to the corresponding mono-model finite-element results.

model ($\alpha_2 = 0.98$); (iii) both L^2 and H^1 (with $\tilde{l} = l_{\rm el}$) operators are adopted. Table III presents the transverse displacement and the normal and shear stress components for a symmetric $[0/90/0]$ plate. The number of DOF of variable kinematic FE solutions is also addressed. Multiple models

Table IV. Transverse displacement and stresses for the $[90/0]_2$ plate, variable kinematic multiple models.

	$-10^5 \times u_z$ (m)	σ_{xx} (MPa)	σ_{yy} (MPa)	$-10 \times \sigma_{xz}$* (MPa)	$-10 \times \sigma_{xz}$† (MPa)	DOF
L^2 coupling operator						
LD1–LM4	1.714, −0.63‡	11.13, −0.89	1.794, −0.71	6.051, −1.46	6.051, −1.46	10 248
LD1–LD4	1.717, +0.00	11.15, −0.17	1.796, −0.33	6.090, −0.45	6.099, +0.49	6984
ED2–LD4	1.688, −1.68	11.17, +0.00	1.796, −0.33	6.123, +0.08	6.139, +1.15	5496
ED1–LD4	1.769, +3.02	10.91, −2.32	1.768, −1.88	6.265, +2.40	6.187, +1.94	4752
FSDT–LD4	1.763, +2.67	10.93, −2.14	1.772, −1.60	6.265, +2.40	6.169, +1.64	4504
ED2–ED4	1.668, −1.76	11.20, +0.08	1.778, +0.00	8.259, +0.54	4.926, +0.55	3192
ED1–ED4	1.746, +2.82	10.95, −2.14	1.750, −1.57	8.262, +0.58	4.928, +0.59	2448
FSDT–ED4	1.739, +2.41	10.97, −1.96	1.753, −1.40	8.262, +0.58	4.928, +0.59	2200
H^1 coupling operator						
LD1–LM4	1.761, +2.08	10.97, −2.31	1.775, −1.77	6.131, −0.16	6.131, −0.16	10 248
LD1–LD4	1.746, +1.68	11.09, −0.71	1.780, −1.22	6.128, +0.16	6.047, −0.36	6984
ED2–LD4	1.707, −0.58	11.17, +0.00	1.796, −0.33	6.123, +0.08	6.139, +1.15	5496
ED1–LD4	1.783, +3.84	10.81, −3.22	1.763, −2.16	6.189, +1.16	6.179, +1.81	4752
FSDT–LD4	1.769, +3.02	10.85, −2.86	1.772, −1.66	6.135, +0.27	6.190, +1.99	4504
ED2–ED4	1.685, −0.76	11.16, −0.26	1.773, −0.28	8.237, +0.28	4.913, +0.28	3192
ED1–ED4	1.761, +3.71	10.90, −2.59	1.745, −1.85	8.220, +0.07	4.903, +0.08	2448
FSDT–ED4	1.747, +2.88	10.97, −1.96	1.753, −1.40	8.249, +0.42	4.920, +0.42	2200

*Value at the bottom of the second layer.
†Value at the top of the third layer.
‡Percentage difference with respect to the corresponding mono-model finite-element results.

solutions match the corresponding mono-model results, proving the effectiveness of the Arlequin method in merging domains discretised via finite elements derived from different theories. Results are similar for the two coupling operators. Accurate results are obtained coupling PVD-based and RMVT-based models, that is, LD1–LM4. The number of DOF is significantly reduced. When ED1 or FSDT is adopted as unrefined theory, results may exhibit inconsistent behaviour with respect to the corresponding mono-model results and, being the two models similar, do not differ up to four significant digits. For instance, in the case of ED1–ED4-coupled solution, σ_{xx} is higher than the corresponding mono-model results; see Table I. It should be noticed that, anyway, the difference from ED4 model is less than 1%. This may be due to the first-order model inability to capture the mechanics of the structure. Results in the case of an anti-symmetric $[90/0]_2$ plate are presented in Table IV. For the transverse displacement, a coupling between FSDT or ED1 model and a higher-order one yields overestimated results by about 3% with respect to the correspondent mono-model solution. At least a second-order model should be assumed for the unrefined sub-domain. The difference in the transverse displacement from the mono-model solution when H^1 coupling operator is used may be due to the shift introduced by this operator in bending problems as reported in Guidault and Belytschko [33]. The choice of the unrefined model in the considered cases is of primary importance: if the unrefined model does not model correctly the global response of the plate, results in the refined sub-domain are less accurate.

7. CONCLUSIONS

The Arlequin method has been used to derive a variable kinematic multiple models analysis of plate structures in the framework of a UF. This UF allows deriving several finite elements via a compact notation that does not depend upon the through-the-thickness expansion order, the description approach (ESL or LW) and the type of main unknowns (PVD or RMVT). According to the used UF, Arlequin coupling matrix has been obtained as a fundamental nucleo. The derivation of the coupling matrix in terms of a fundamental nucleo yields a straightforward implementation of the Arlequin method regardless the kinematic assumptions of the coupled theories. Relatively thick composite

plates have been investigated. A localised bending loading has been accounted for. Refined finite elements have been used only in those sub-domains of the structure where a quasi-three-dimensional stress field occurs. The proposed coupled models have been validated towards mono-models solutions and a three-dimensional elasticity approach. It has been shown that the Arlequin method proves to be an effective approach to couple sub-domains of the structure modelled with finite elements having different kinematics and/or variational principle. Two coupling operators have been accounted for. H^1 coupling may yield inaccurate results if the lower-order model lacks in capturing the mechanics of the structure. This is emphasised by high values of the length parameter $\tilde{l}$. In these cases, L^2 coupling operator should be preferred. The size of the superposition zone has no significant effect on the accuracy of the coupling. In order to reduce the computational cost, the coupling volume should be reduced as much as possible. Accurate results have been obtained in the refined part of the model with a significant reduction of the total number of degrees of freedom and, therefore, of the computational cost. The proposed variable kinematic multiple models approach is of particular interest for practical cases (for instance, free edges, concentrated loads, cut-outs, delaminations and failures) in which high gradients or singularities occur in localised regions. Accurate modelling of the mechanics of these regions requires a local refinement of the solution.

REFERENCES

1. Ben Dhia H. Multiscale mechanical problems: the Arlequin method. *Comptes Rendus de l'Academie des Sciences Series IIB Mechanics Physics Astronomy* 1998; **326**(12):899–904.
2. Ben Dhia H. Numerical modelling of multiscale problems: the Arlequin method. *CD Proceedings of ECCM'99*, Munchen, 1999.
3. Ben Dhia H. Further insights by theoretical investigations of the multiscale Arlequin method. *International Journal for Multiscale Computational Engineering* 2008; **6**(3):215–232.
4. Ben Dhia H, Rateau G. The Arlequin method as a flexible engineering tool. *International Journal for Numerical Methods in Engineering* 2005; **62**(11):1442–1462.
5. Kirchhoff G. Über das gleichgewicht und die bewegung einer elastischen scheibe. *Journal für die reine und angewandte Mathematik* 1850; **40**:51–88.
6. Reissner E. The effect of transverse shear deformation on the bending of elastic plates. *Journal of Applied Mechanics* 1945; **12**(2):69–77.
7. Mindlin RD. Influence of rotatory inertia and shear on flexural motions of isotropic, elastic plates. *Journal of Applied Mechanics* 1951; **18**:31–38.
8. Carrera E. C_z^0 requirements—models for the two dimensional analysis of multilayered structures. *Composite structures* 1997; **37**(3–4):373–383.
9. Kapania RK, Raciti S. Recent advances in analysis of laminated beams and plates, part I: shear effects and buckling. *AIAA Journal* 1989; **27**(7):923–934.
10. Kapania RK, Raciti S. Recent advances in analysis of laminated beams and plates, part II: vibrations and wave propagation. *AIAA Journal* 1989; **27**(7):935–946.
11. Noor AK, Burton WS. Assessment of shear deformation theories for multilayered composite plates. *Applied Mechanics Reviews* 1989; **41**:1–18.
12. Reddy JN, Robbins Jr DH. Theories and computational models for composite laminates. *Applied Mechanics Review* 1994; **47**(6):147–169.
13. Carrera E. Historical review of Zig-Zag theories for multilayered plates and shells. *Applied Mechanics Reviews* 2003; **56**:287–308.
14. Hu H, Belouettar S, Potier-Ferry M, Daya EM. Review and assessment of various theories for modeling sandwich composites. *Composite Structures* 2008; **84**(3):282–292.
15. Carrera E. A class of two dimensional theories for multilayered plates analysis. *Atti Accademia delle Scienze di Torino, Memorie Scienze Fisiche* 1995; **19–20**:49–87.
16. Reissner E. On a certain mixed variational theorem and a proposed application. *International Journal for Numerical Methods in Engineering* 1984; **20**:1366–1368.
17. Carrera E. Theories and finite elements for multilayered plates and shells: a unified compact formulation with numerical assessment and benchmarking. *Archives of Computational Methods in Engineering* 2003; **10**(3):215–296.

18. Fish J, Pan L, Belsky V, Gomaa S. Unstructured multigrid method for shells. *International Journal for Numerical Methods in Engineering* 1996; **39**(7):1181–1197.
19. Fish J. The *s*-version of the finite element method. *Computers and Structures* 1992; **43**(3):539–547.
20. Fish J, Markolefas S. Adaptive *s*-method for linear elastostatics. *Computer Methods in Applied Mechanics and Engineering* 1993; **103**:363–396.
21. Park KC, Felippa CA. A variational principle for the formulation of partitioned structural systems. *International Journal for Numerical Methods in Engineering* 2000; **47**:395–418.
22. Blanco PJ, Feijoo RA, Urquiza SA. A variational approach for coupling kinematically incompatible structural models. *Computer Methods in Applied Mechanics and Engineering* 2008; **197**:1577–1620.
23. Brezzi F, Marini LD. The three-field formulation for elasticity problems. *GAMM Mitteilungen* 2005; **28**:124–153.
24. Hu H, Belouettar S, Potier-Ferry M, Daya EM. Multi-scale modelling of sandwich structures using the Arlequin method. Part I: linear modelling. *Finite Elements in Analysis and Design* 2008; **45**(1):37–51.
25. Hu H, Belouettar S, Potier-Ferry M, Daya EM, Makradi A. Multi-scale nonlinear modelling of sandwich structures using the Arlequin method. *Composite Structures* 2010; **92**(2):515–522.
26. Biscani F, Giunta G, Belouettar S, Carrera E, Hu H. Variable kinematic beam elements coupled via Arlequin method. *Composite Structures* 2011; **93**(2):697–708.
27. Reddy JN. *Mechanics of Laminated Composite Plates and Shells*, 2nd ed, Theory and Analysis. CRC Press: Boca Raton, 2004.
28. Carrera E, Brischetto S. Analysis of thickness locking in classical, refined and mixed multilayered plate theories. *Composite Structures* 2008; **82**(4):549–562.
29. Carrera E, Giunta G. Hierarchical evaluation of failure parameters in composite plates. *AIAA Journal* 2009; **47**(3):692–702.
30. Reissner E. On a mixed variational theorem and on shear deformable plate theory. *International Journal for Numerical Methods in Engineering* 1986; **23**:193–198.
31. Bathe KJ. *Finite Element Procedures*. Prentice Hall: New Jersey, 1996.
32. De Masi L, Carrera E. Classical and advanced multilayered plate elements based upon PVD and RMVT. Part 1. Derivation of finite element matrices. *International Journal for Numerical Methods in Engineering* 2002; **55**:191–231.
33. Guidault PA, Belytschko T. On the L2 and the H1 couplings for an overlapping domain decomposition method using Lagrange multipliers. *International Journal for Numerical Methods in Engineering* 2007; **70**(3):322–350.
34. Pagano NJ. Exact solutions for rectangular bidirectional composites and sandwich plates. *Journal of Composites Materials* 1970; **4**:20–34.